A Simplified Mass Transfer Model for Visual Pigments in Amphibian Retinal Cone Outer Segments - Supplemental Material

Paul W. Weber,[†] Laurens E. Howle,[†,‡,*] Mark M. Murray,[§] and Joseph M. Corless[¶]

[†]Department of Mechanical Engineering and Materials Science, Duke University, Durham, North Carolina; [‡]Center for Nonlinear and Complex Systems, Duke University, Durham, North Carolina; [§]Department of Mechanical Engineering, United States Naval Academy, Annapolis, Maryland; [¶]Departments of Cell Biology, Neurobiology and Ophthalmology, Duke University Medical Center, Durham, North Carolina
[*]Correspondence: laurens.howle@duke.edu

In this supporting material document, we first derive an expression for the material velocity predicted in the plasmalemma from the recycling component of the model. This is followed by a discussion of analytic solution attempts to the problem. A discussion of the results obtained by applying perturbation methods to the problem is then presented. A discussion of the estimated numerical value of the mass transfer coefficient, h_m, is next, followed by a note on the comparison of this 1-D model to a full 3-D recycling model.

This supporting material document also contains three figures (Figs. S1, S2, and S3) and an addendum to Table 1. Fig. S1 explains the error that is accepted due to approximations made in the model, and Fig. S2 shows the numerical results of the perturbation method. Fig. S3 shows relevant geometry used to estimate h_m. The addendum to Table 1 describes how the numerical values reported in Table 1 were obtained.

Derivation of Plasmalemma Velocity

We begin by writing an expression for the incremental volume of a given disc region, labeled ΔV in Fig. 3:

$$\Delta V = \pi r^2 \Delta x \phi \qquad \text{(S1)}$$

where Δx is the incremental disc thickness as labeled in Fig. 3, ϕ is the non-void fraction, and the radius of the cone, r, is given by:

$$r = r_b + \frac{x}{L}\left(r_t - r_b\right) \qquad \text{(S2)}$$

In Eq. S2, r_t is the radius at the cone tip, r_b is the radius at the cone base, L is the COS length and x is the axial distance from the cone base. Next, the change in the incremental volume ΔV with respect to time (which gives a volume flow rate) at any point x along the disc region must be calculated. This is necessary because principles of mass conservation dictate that material volume exiting the disc region must enter the plasmalemma region. Taking the time derivative of Eq. S1, applying the chain rule, substituting previously defined values, and carrying out the derivatives gives:

$$\begin{aligned}\frac{d(\Delta V)}{dt} &= \frac{d(\Delta V)}{dx}\frac{dx}{dt} = \frac{d(\Delta V)}{dr}\frac{dr}{dx}\frac{dx}{dt} \\ &= \frac{d\left(\pi r^2 \Delta x \phi\right)}{dr}\frac{d}{dx}\left(r_b + \frac{x}{L}\left(r_t - r_b\right)\right)\frac{dx}{dt} \\ &= \frac{2\pi r \Delta x \phi\left(r_t - r_b\right)}{L}\frac{dx}{dt}\end{aligned} \tag{S3}$$

The quantity $\frac{dx}{dt}$ in Eq. S3 is recognized as the disc displacement velocity u_1 from Table 1. Making this substitution and dividing by the cross-sectional area of the material flow out of the disc region and into the plasmalemma $W\Delta x$ gives:

$$\frac{d(\Delta V)}{dt}\frac{1}{W\Delta x} = \frac{2\pi r \Delta x \phi\left(r_t - r_b\right)}{LW\Delta x}\frac{dx}{dt} = \frac{2\pi r \phi\left(r_t - r_b\right)}{LW}u_1 \tag{S4}$$

The quantity $\frac{d(\Delta V)}{dt}$ is the volume flow rate out of the disc region and into the plasmalemma at any given point x. When scaled by the cross-sectional area of the flow out of the disc region, $W\Delta x$, the result is the velocity out of the disc region, denoted as v. Equation S4 is the expression for v, and by substituting the definition of r from Eq. S2, the final result for v is:

$$v = \frac{2\pi\phi u_1\left(r_t - r_b\right)}{LW}\left[r_b + \frac{x}{L}\left(r_t - r_b\right)\right] \tag{S5}$$

Note that since $r_b > r_t$, $\phi > 0$, $u_1 > 0$, $L > 0$, $W > 0$, and $0 \le x \le L$, v will be negative across the entire domain. The negative value of v physically represents the fact that bulk flow of material is always flowing *out* of the disc region and *into* the plasmalemma during recycling (5).

Now that the material velocity exiting the disc region at any point x has been obtained in Eq. S5, we may proceed to derive an expression for the material velocity in the plasmalemma, u_2 (recall that u_1 is the disc displacement velocity). Two assumptions are made at this point; the first is that the flow in the plasmalemma is driven solely by the material exiting the disc region, and the second is that the plasmalemma velocity at the tip of the COS is zero. The plasmalemma flow velocity at any point x may be calculated by integrating the flow into the plasmalemma region (which is the negative of the flow out of the disc region), and applying appropriate boundary conditions. The equation which represents this is:

$$u_2 WT = -\int v W dx \tag{S6}$$

In Eq. S6, WT is the cross-sectional area through which u_2 flows, while Wdx is the cross-sectional area through which v flows. Substituting known values and carrying out the integration gives:

$$u_2 WT = -\int \frac{2\pi\phi u_1 (r_t - r_b)}{LW}\left[r_b + \frac{x}{L}(r_t - r_b) \right] W dx$$
$$= -\frac{2\pi\phi u_1 (r_t - r_b)}{L}\int \left[r_b + \frac{x}{L}(r_t - r_b) \right] dx \qquad \text{(S7)}$$
$$= -\frac{2\pi\phi u_1 (r_t - r_b)}{L}\left[r_b x + \frac{x^2}{2L}(r_t - r_b) + C^{st} \right]$$

The arbitrary constant of integration C^{st} in Eq. S7 may be determined by requiring that $u_2 = 0$ at $x = L$. This condition is physically motivated by the fact that material may only flow out of the plasmalemma at the left side of the domain (base, $x = 0$), so the right side of the domain (tip) at $x = L$ is a wall through which no material may pass and therefore the material velocity is zero at that point. Applying this physical restraint in Eq. S7 yields:

$$0 = r_b L + \frac{L^2}{2L}(r_t - r_b) + C^{st} \rightarrow C^{st} = -\frac{L}{2}(r_t + r_b) \qquad \text{(S8)}$$

Substituting the expression for C^{st} from Eq. S8 into Eq. S7 yields:

$$u_2 = -\frac{\pi\phi u_1 (r_t - r_b)}{LWT}\left[2r_b x + \frac{x^2}{L}(r_t - r_b) - L(r_t + r_b) \right] \qquad \text{(S9)}$$

The value of u_2 in Eq. S9 is negative across the entire domain except for the point $x = L$ where it is zero due to the boundary condition previously mentioned. With this continuum expression for the plasmalemma material velocity, a simplified mass transfer model for the label density may be derived.

Analytic Solution Attempts

Ideally, we would like to have an analytic solution to the system of Eqs. 13. Analytic solutions have numerous advantages, the most notable being gain of physical insight into the problem and ease of calculating results. In our attempt to find an analytic solution to this problem, we first used numeric solution methods to gain some preliminary insight. The most important insight gained numerically was that the solution to the approximate Eqs. 15 was indistinguishable from the full system Eqs. 13 for earlier times. So, if an analytic solution to the approximate system Eqs. 15 may be found, it will be of as much value as a solution to the full system Eqs. 13 for early times. From inspection of the two equation systems, it seems that if an analytic solution does indeed exist, it will be much easier to determine for the approximate system than for the full system since there are less terms to deal with. Also, it is of note that if an analytic solution cannot be found for the approximate system Eqs. 15, then it is unlikely that it will be found for the full system Eqs. 13, so it seems natural to attempt a solution to the approximate system first.

There is one analytic solution that is immediately apparent, and that is the steady-state solution. By setting all time derivatives to zero in Eqs. 15, then adding the two equations, we get the ODE

$$\frac{d^2 \rho_2^*}{dx^{*2}} = 0 \qquad \text{(S10)}$$

which is subject to the same boundary conditions as before. Solving Eq. S10 and using the result to solve for the disc region yields the steady-state solution

$$\left.\begin{aligned}\rho_2^* &= 1\\ \rho_1^* &= \phi\end{aligned}\right\rangle \text{as } t \to \infty \tag{S11}$$

The following solution methods to obtain an analytic result were attempted, none of which were successful: direct substitution, approximating the cone geometry as a rectangle to yield a constant-coefficient equation, similarity solution (S1), reduction of order/state-space, computer algebra system, and regular perturbation theory (28). However, regular perturbation theory did yield one useful insight. For this problem, the parameter $\varepsilon = \dfrac{TD}{h_m L^2}$ in system Eqs. 15 is small compared to the others, so a power series solution was assumed such that

$$\begin{aligned}\rho_2^*(x,t,\varepsilon) &= \sum_{i=0}^{\infty} \rho_{2_i}^*(x,t)\varepsilon^i\\ \rho_1^*(x,t,\varepsilon) &= \sum_{i=0}^{\infty} \rho_{1_i}^*(x,t)\varepsilon^i\end{aligned} \tag{S12}$$

When the perturbation method was applied to system Eqs. 15, the resulting partial differential equation obtained (with initial and boundary conditions) was

$$\begin{aligned}&\left[1+\frac{\phi\pi}{WT}\left(r_b + x\left(r_t - r_b\right)\right)^2\right]\frac{\partial \rho_2^{(0)}}{\partial t} = \frac{\partial^2 \rho_2^{(0)}}{\partial x^2},\\ &\rho_2^{(0)}(0,t) = 1, \quad \frac{\partial \rho_2^{(0)}(1,t)}{\partial x} = 0, \quad \rho_2^{(0)}(x,0) = 0\\ &\rho_1^{(0)} = \phi\rho_2^{(0)}\end{aligned} \tag{S13}$$

which is a non-constant coefficient, uncoupled partial differential equation. No analytic solution was found for Eqs. S13, although a numeric study (see Fig. S2) showed that they did yield results of acceptable accuracy for times greater than 15 min of physical time. The advantage gained by using Eqs. S13 is that if one is only interested in later times, numeric solutions for an uncoupled problem such as that in Eqs. S13 are much easier to program than solutions for the full, coupled system of Eqs. 13 or Eqs. 15.

Perturbation Solution Results

Fig. S2 shows a comparison of the numerical solution of the full system Eqs. 13 with the numerical solution of the system obtained by perturbation methods Eqs. S13 for different times. Recall that the system Eqs. S13 was obtained by only considering the leading term in the power series Eqs. S12. For the same reasons mentioned previously, the first parameter set corresponding to the onset of the light cycle was used for this perturbation method study. As seen in Fig. S2*A-B,* the perturbation solution is very poor for early time regimes. This is not surprising due to the fact that during Stage 1 of the mass transfer process, diffusion in the plasmalemma is the principal factor and in Stage 2 the mass transfer coefficient is the principal factor, but the first term in the power series does not contain the diffusion constant or mass transfer coefficient as a parameter. This is due to the definition of the perturbation parameter

$\varepsilon = \frac{TD}{h_m L^2}$, which contains the effects of the diffusion constant and mass transfer coefficient and only appears in the second and higher terms of the power series Eqs. S12. Fig. S2*C-E* show that the perturbation approximation improves as time increases, but tends to under-predict the density profile; depending on the accuracy required, these solutions may be acceptable. Fig. S2*F* shows that the perturbation solution slightly worsens as time increases, but the difference in accuracy between the perturbation solution at 2 h and the solution without advection (Fig. 7*F*) at 2 h is negligible. It is also of note that the perturbation method predicts the correct steady-state solution. Finally, very large gains in computational speed are gained by using the perturbation solution, due to the fact that the system is uncoupled and also produces a diagonal matrix, which allows for the exploitation of computationally efficient algorithms.

Estimation of Mass Transfer Coefficient, h_m

We derive an approximation for h_m by considering the species flux into and out of the plasmalemmal control area (PL_2; area = W * d) associated with disc 2, as illustrated in Fig. S3. We select this level for analysis in order to avoid the need to deal with the half-disc (single membrane) attached to the basal-most disc (disc 1) along its open margin segment and also connected to the connecting cilium.

The flux of label into control area PL_2 is F_2, arriving via diffusion from the lower control area PL_1. Net diffusion of label into control area PL_2 can follow two available paths: direct axial diffusion to the adjacent control area PL_2 , and axio-lateral diffusion (F_d) into disc 2 via the two saddle points (SP). The relative amounts of label transported to these two sites will be related to the aperture for entry into those sites. For axial diffusion, the aperture is the width of the plasmalemma (W = 2.1 μm). For lateral diffusion into disc 2, the aperture for diffusion is twice the aperture for each saddle point. The axial length (diameter) of the saddle point region is less than d, and is estimated to be 0.5 * d from electron microscopic data (e.g., see Fig. 1). Thus, for two saddle points, the aperture is d (dashed lines in PL_2).

Given the value of the diffusion constant D = 0.5 $\mu m^2/s$ (Table 1), the root-mean-square displacement of labeled opsins is 0.3 μm/s (24). This value provides a close approximation for the labeled species flux in the axial direction. The axial diffusion front from x = 0 will reach x = d at $t_1 = \sim 0.115$ s (d = 0.3 μm/s * t), and x = 2d at $t_2 = \sim 2*t_1$. At t_1, the concentration of labeled species in PL_2 and disc 2 will be zero. During the time interval ($t_2 - t_1$), some label arriving from control area PL_1 will have also diffused laterally through each saddle point to the same distance d, if the height of this diffusion strip is maintained at d/2. The number of labeled opsins transported into this axial segment of the COS [x = d to x = 2d] will be n_2, and these will be distributed over an area A_2 equal to the control area PL_2 [W * d = 0.0727 μm^2] plus the area populated via the two saddle points [2 * (0.5 * d) * d = d^2 = 0.0012 μm^2], or A_2 = 0.0739 μm^2. The number of labeled opsins in PL_2 will be $n_{PL2} = n_2 * (W * d) / A_2 = 0.9838 * n_2$, and the number entering disc 2 will be $n_{d2} = n_2 * d^2 / A_2 = 0.0162 * n_2$. Thus, given the initial label density gradient between control area PL_1 and disc 2 (label density = 0), the relative flux of labeled opsins into disc 2 is small (0.0162) compared to that transferred to PL_2. This small fractional transfer is governed primarily by the dimensions and geometry of the control area, and

by the difference in label concentration. The coefficient derived (0.0162 $\mu m / s$) provides one estimate of h_m.

A second estimate for lateral diffusion into disc 2 from PL_2 takes into account the curved shape of each saddle point, as illustrated in PL_3. Approximating this local curvature as a semicircle of diameter d/2, the entry aperture for disc 2 will be (π/2)*(d/2). Thus, the total length of the diffusion interface for PL_2 will be W + 2*(π/2)*(d/2) = W + π * (d/2). The estimate of h_m using these values is 0.02523 $\mu m / s$. Given potential errors in estimates for W, d the saddle point height and actual SP curvature, a reasonable approximation, based upon saddle point geometry and topology is the larger value: $h_m = 0.025\ \mu m / s$.

A Note on Recycling

The detection of label in newly formed basal discs is confronted with an additional hurdle that emerges when comparing the 1-D model with the full 3-D recycling model. The 1-D model applies a constant concentration of label across the base of the COS, i.e., to both the disc core region and to the plasmalemmal region. Thus, the curves in Fig. 5 provide upper estimates for the label density in the disc region. But in the 1-D model, only three components of advection are operative: apical displacement of discs, flow of disc membrane components to the plasmalemma as the discs become smaller, and advective flow of the older disc components in the plasmalemma towards the base of the COS (Fig. 3, block arrows). Not included is a fourth component of advective flow that directs recycled opsins and lipids accumulating around the basal plasmalemma to the newly forming disc. During the early stages of system evolution, most of these recycled opsins are unlabeled, and the recycling model predicts that they will mix in the basal plasmalemma region with new labeled opsins (arriving via the connecting cilium). This diluted mixture is what would primarily characterize a reduced labeling density of new discs. In contrast, we know from comparing label density distributions with and without advection (Fig. 6) that during the first 30 min of system evolution, advection has no discernible effect on label density distribution in either the plasmalemma or disc core region, and even thereafter, the effect is small. Basal advection of the plasmalemma is just much slower than the apical diffusion of opsin. Thus, we expect that the labeled opsin density distribution along the plasmalemma will be established basically as calculated. In this view, the recycling model predicts that the new basal disc will develop a density of label that is significantly less than that available near the connecting cilium for axial diffusion along the plasmalemma. However, axial diffusion along the plasmalemma is rapid and quickly transfers label to discs in the basal region. The rate of accumulation of new basal discs is very slow and their label density will quickly become dictated by the label density distribution established along the plasmalemma.

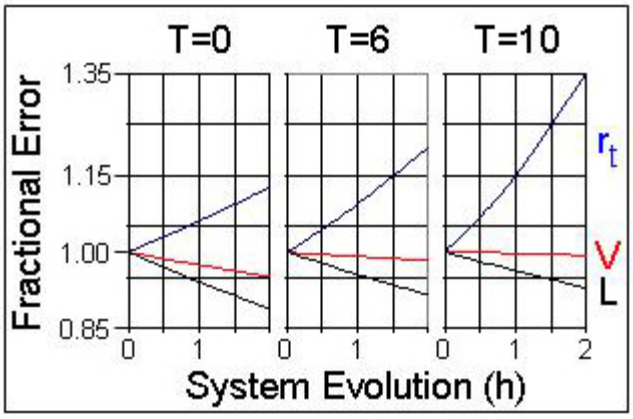

FIGURE S1 Error analysis for COS model during system evolution. In this advection-diffusion model, the length of the COS (L) and its tip radius (r_t) remain constant during the calculation of density distributions, whereas the COS increases in length at velocity u_1 and the tip radius continuously decreases. Thus, as the system evolves over time, there is progressive divergence of in vivo parameter values from model parameters. For the three starting time points in the light cycle evaluated (Table 1), the errors in these parameters are evaluated as the starting value divided by the value at later time points. The evolution of frustum volume (V) is also evaluated. In general, the model underestimates length and volume over time, and overestimates tip radius. However, at the 2-h time points, two model parameters represent in each case a high percentage of calculated *in vivo* values: V = 95%, 98.1% and 99.3%; L = 88.8%, 91.6% and 92.8%. While the tip radius diverges increasingly at longer COS starting lengths, its effect on estimating COS volume is quite small due to the converging geometry of the COS tip. This analysis indicates that system evolution of the model is robust, involving 100-95% of the COS volume during the 2-h evolution periods, and that model accuracy is greater at longer COS starting lengths.

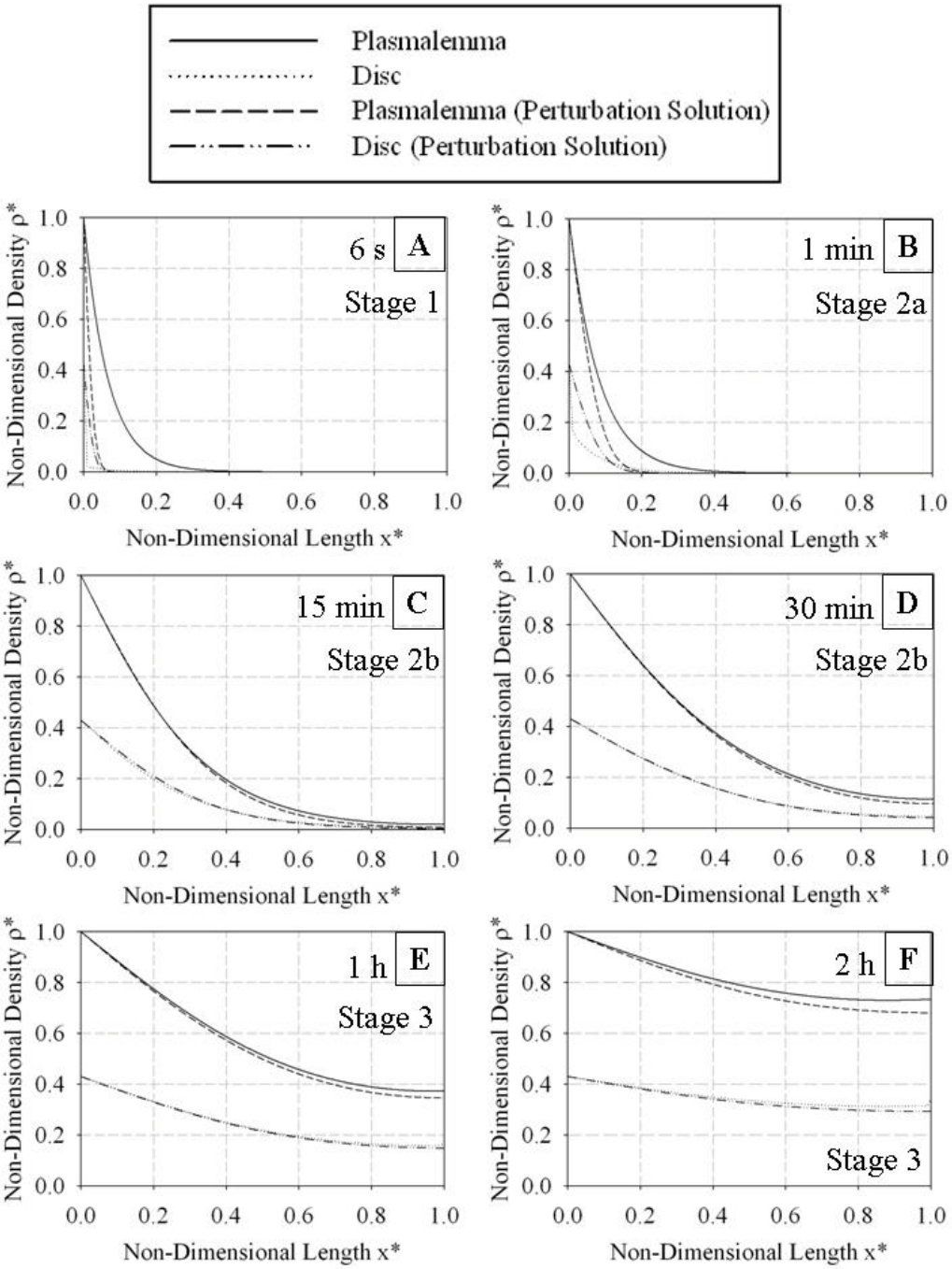

FIGURE S2 Comparison of solution with advection versus perturbation solution for (a) 6 s (b) 1 min (c) 15 min, (d) 30 min, (e) 1 h, and (f) 2 h of system evolution. Parameters used in the solution represent the onset of the light cycle (L_1 , r_{t1} in Table 1). Perturbation methods result in a significant decrease in solution time. The perturbation solution is inaccurate for early times and is of greatest accuracy for times of 15 min – 1 h; the solution at the latest time of 2 h may be acceptable depending upon accuracy required.

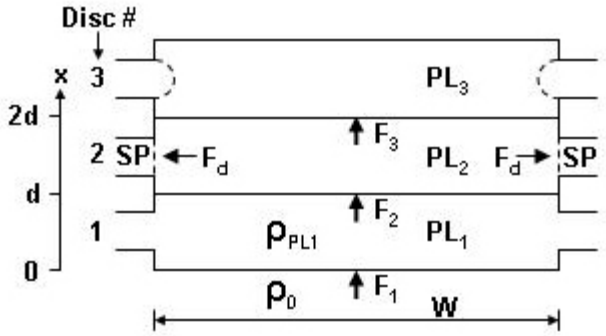

FIGURE S3 Plasmalemma control areas. The label density present at the base of the COS (x = 0) is the reference value ρ_0. At $t = t_1$, label density within PL_1 is ρ_{PL1}, and label density within PL_2 and disc 2 and is also zero. The height of each control area is d = 0.0346 μm, the axial disc repeat period and its width is the arc length of the plasmalemma W = 2.1 μm (Table 1). In PL_2, the diffusion aperture through the saddle point (SP) into disc 2 is shown as a dashed vertical line. In PL_3, the curvature of the saddle point in this plane is approximated as a semicircle (dashed line).

EXPLANATORY NOTES FOR TABLE 1:

[1] The lateral diffusion of visual pigments (rhodopsin, porphyropsin) have been studied in a number of animal species and isolated disc preparations (24, 25, S2 – S6). Values of *D* vary between 3.0 – 5.5 x 10-9 cm^2/s. The value selected is representative of amphibian photoreceptors.

[2] Based on data for the African clawed frog (*Xenopus laevis*) reported by Eckmiller (16, 17). The average basal diameter is 4.2 μm and does not change significantly between the time of light onset and light offset, i.e., during the period of COS elongation.

[3] For *Xenopus* maintained on 12 h light : 12 h dark cycles, Eckmiller (16, 17) reported that the mean COS length at light onset was 3.8 μm and increased to 6.7 μm over the next 12 h. At an axial density of 45 discs (lamellae) per micron in fixed and embedded tissue, the COS increased in length from an average of n = 171 discs to n = 301 discs over the 12 h light interval, or an increase of Δn = 130 lamellae over 720 minutes. This increase in length is basically monotonic. In order to approximate the lengths and changes in length *in vivo* compared to measurements from fixed and embedded specimens, we need an estimate of the axial spacing, *d*, of COS discs *in vivo*. While not a directly available parameter, we have estimated *d* for COSs by scaling Nilsson's ROS disc spacing data (2) to that obtained by x-ray (S7) and neutron diffraction data of fresh tissue, and applying that scale factor to his axial spacing data for COSs. We estimate that for amphibian COSs, *d* = 34.6 nm, which is close to the estimate from freeze-etch data (5, Fig. 7: 35.0 nm). Thus, over the 12 h light period, *Xenopus* COSs increase in length from 5.92 μm (=171**d*) to 10.42 μm (=301**d*). We equate this axial growth rate with the axial rate at which discs are added and advanced apically in the COS: one disc is added every 5.54 min. From Eckmiller's image data, we also estimated that the conical generator angle *in vivo* is α = 9.5°.

The radius (r_t) of the COS tip at different COS lengths (L) was estimated from the formula: $\tan\alpha = (r_b - r_t)/L$, where $L = n \cdot d$.

The average increase in *Xenopus* COS length (2.9 μm) during the 12-hour light period observed by Eckmiller (16, 17) agrees closely with the estimated length increase in lizard COSs (~2.7 μm) reported by Bernstein et al. (S8). Both values are significantly higher than early estimates inferred from analyses of the sizes of disk packets shed from COS tips and phagocytized by the retinal pigment epithelium (15, S9), where the frequency of shedding events was uncertain.

[4] The non-void membrane fraction of each axial repeat interval is represented by the two membranes of each disc. The thickness of each membrane, i.e., the thickness of the layer in which lateral diffusion occurs, is set equal to 7.5 nm, the length of the bovine rhodopsin molecule (S10) measured perpendicular to disc membrane and centered on the lipid bilayer (~4.0 nm thick). The non-void dimension of the two disc membranes is 2 * 7.5 nm = 15.0 nm. We base the non-void fraction of each disc repeat period on an average value for the disc spacing d=34.6 nm: $\varphi = 15.0/34.6 = 0.43$. The *in vivo* variation in COS disc spacings is not established, but analyses of x-ray diffraction data from ROSs (S7) suggests a possible range: for an average axial disk spacing of 29.5 nm, the lattice nearest neighbor spacing has a variation of ±1.9 nm (6.44%). Because the axial disc repeat distance in COSs appears larger than in ROSs, we expect larger variation. The plasmalemma thickness (T) is set equal to the thickness of a disc membrane (7.5 nm) based on EM images.

[5] Plasmalemma width is estimated from the arc length of the closed margin of COS discs (5), which is ~ 2.1 μm and approximately constant along the COS.

SUPPORTING MATERIAL REFERENCES

S1. Bejan, A. 1993. Heat Transfer. John Wiley & Sons, Inc., New York.

S2. Poo, M., and R.A. Cone. 1974. Lateral Diffusion of Rhodopsin in the Photoreceptor Membrane. Nature. 247: 438-441.

S3. Wey, C.L., R.A. Cone, and M.A. Edidin. 1981. Lateral Diffusion of Rhodopsin in Photoreceptor Cells Measured by Fluorescence Photobleaching and Recovery. Biophys. J. 33: 225-232.

S4. Takezoe, H., and H. Yu. 1981. Lateral Diffusion of Photo-Pigments in Photoreceptor Disk Membrane-Vesicles by the Dynamic Kerr Effect. Biochemistry-US. 20: 5275-5281.

S5. Drzymala, R.E., H.L. Weiner, C.A. Dearry, and P.A. Liebman. 1984. A Barrier to Lateral Diffusion of Porphyropsin in Necturus Rod Outer Segment Disks. Biophys. J. 45: 683-692.

S6. Kaplan, M.W. 1984. Rhodopsin Lateral Diffusion as a Function of Rod Outer Segment Disk Membrane Axial Position. Biophys. J. 45: 851-853.

S7. Schwartz, S., J.E. Cain, E.A. Dratz, and J.K. Blasie. 1975. An Analysis of Lamellar X-Ray Diffraction from Disordered Membrane Multilayers with Application to Data from Retinal Rod Outer Segments. Biophys. J. 15: 1201-1233.

S8. Bernstein, S.A., Breding, D.J., and Fisher, S.K. 1984. The Influence of Light on Cone Disk Shedding in the Lizard, *Sceloporus occidentalis*. J. Cell Biol. 99: 379-389.

S9. Young, R.W. 1978. Daily Rhythm of Shedding and Degradation of Rod and Cone Outer Segment Membranes in Chick Retina. Invest. Ophth. Vis. Sci. 17: 105-116.

S10. Palczewski, K., T. Kumasaka, T. Hori, C.A. Behnke, H. Motoshima, et al. 2000. Crystal Structure of Rhodopsin: A G Protein-Coupled Receptor. Science. 289: 739-745.